The Interaction Between Coronal Mass Ejections and Streamers: A Statistical View over 15 Years (1996 – 2010)

O. Floyd · P. Lamy · A. Llebaria

Abstract We report on the statistical analysis of the interaction between coronal mass ejections (CMEs) and streamers based on 15 years (from 1996 to 2010 inclusive) of observation of the solar corona with the LASCO-C2 coronagraph. We used synoptic maps and improved the method of analysis of past investigations by implementing an automatic detection of both CMEs and streamers. We identified five categories of interaction based on photometric and geometric variations between the pre- and post-CME streamers: "brightening", "dimming", "emergence", "disappearance", and "deviation". A sixth category, "no change", included all cases where none of the above variations is observed. A "global set" of 21 242 CMEs was considered as well as a subset of the 10 % brightest CMEs (denoted "top-ten") and three typical periods of solar activity: minimum, intermediate, and maximum. We found that about half of the global population of CMEs are not associated with streamers, whereas 93 % of the 10 % brightest CMEs are associated. When there is a CME-streamer association, approximately 95 % of the streamers experience a change, either geometric or radiometric. The "no change" category therefore amounts to approximately 5 %, but this percentage varies from 1 – 2 % during minimum to 7 – 8 % during intermediate periods of activity; values of 3 – 5 % are recorded during maximum. Emergences and disappearances of streamers are not dominant processes; they constitute 16 – 17 % of the global set and 23 % (emergence) and 28 % (disappearance) of the "top-ten" set. Streamer deviations are observed for 57 % and 70 % of, respectively, the global set and "top-ten" CMEs. The cases of dimming and brightening are roughly equally present and each case constitutes approximately 30 – 35 % of either set, global or "top-ten".

Keywords Corona, structures · Coronal mass ejections

O. Floyd · P. Lamy (✉) · A. Llebaria
Laboratoire d'Astrophysique de Marseille, UMR 7236, CNRS/Aix-Marseille Université, 38 rue Frédéric Joliot-Curie, 13388 Marseille cedex 13, France
e-mail: philippe.lamy@oamp.fr

O. Floyd
e-mail: olivier.floyd@oamp.fr

A. Llebaria
e-mail: antoine.llebaria@oamp.fr

1. Introduction

The question of the relationship of coronal mass ejections (CMEs) to streamers dates back to their early observations with space coronagraphs and subsequent efforts to understand their origin. Based on observations with the *Solwind* instrument, Howard *et al.* (1985) introduced the terminology of "streamer blowout" to denote the events where the occurrence of a CME essentially removes a pre-existing streamer. The *Solar Maximum Mission* (SMM) corona-graph confirmed this process (Illing and Hundhausen, 1986) and a statistical analysis of the data led Hundhausen (1993) to the generally accepted notion that CMEs are associated with the streamer belt. Introducing synoptic maps to study this association for the first time, he found that approximately half of the CMEs in 1984 produced a conspicuous disruption of the pre-existing structure, thus confirming the idea that CMEs originate in the destabiliza-tion of large-scale magnetic fields in a streamer (Low, 1983; Wolfson, Illing, and Conover, 1987; Hundhausen, 1987).

Observations with the soft X-ray telescope on the *Yohkoh* spacecraft completed the pic-ture by showing that a helmet streamer could reform by magnetic reconnection after giving the way to a CME (Hiei, Hundhausen, and Sime, 1993). McAllister and Hundhausen (1996) further established a relation between *Yohkoh* coronal arcade events, coronal streamers, and CMEs revealing that 73 % of these arcade events (known to be proxies for CMEs) are asso-ciated with the streamer belt.

The *Large Angle Spectrometric COronagraph* (LASCO; Brueckner *et al.*, 1995) with its superior sensitivity and record longevity allows to cast more light on the CME-streamer relation as compared to the past studies based on *Solwind* and SMM data. Subramanian *et al.* (1999) used LASCO-C2 data spanning a period of two years from the 1996 minimum through the rising phase of Cycle 23 (June 1998) to build synoptic maps of the white light corona at 2.5 $R_\odot$ onto which they superimposed the positions of CMEs recorded directly on the C2 images. They identified four types of interactions and found that approximately 35 % of the observed CMEs bear no relation to the pre-existing streamer belt, 46 % have no effect on the observed streamer, even though they appear to be related to it, and only 16 % disrupt the streamer. Llebaria *et al.* (2006) extended this work by considering three periods spanning the first ten years of LASCO operation (1996 to 2005) and typical of minimum, intermediate, and high activity. They introduced five classes of interaction based on photometric (brightening versus dimming) and geometric changes of the streamer belt occurring after a CME, further distinguishing slow and fast events. Concerning the influence of rising solar activity, they noticed a sharp decrease of the proportion of CMEs having no effect, a pronounced increase of the proportion of CMEs reinforcing the streamer belt, and a decrease of the proportion of CMEs deviating the streamers. Concerning the influence of the CME velocity, they noticed that ≈ 50 % of the fast CMEs have no effect on the streamer belt whereas all slow CMEs affect it one way or the other.

Odstrcil and Pizzo (1999) and Mancuso and Raymond (2004) have shown that CMEs have very significant interactions with streamer belt structures. Cho *et al.* (2011) suggested that the CME-streamer interaction is one of the two main mechanisms able to generate multiple type II radio bursts.

There is a general consensus that the origin of CMEs lies in the catastrophic loss of equilibrium of a magnetic configuration, with the release of the stored energy and helicity and a subsequent reconfiguration of the disrupted fields, magnetic reconnection playing a fundamental role in the whole process. However, there are conflicting views on the process at work. In the "traditional" picture of a CME eruption as suggested by Low (1996), a flux rope underneath a streamer is stressed by some mechanisms to the point of instability and

ejection of the plasma bubble that surrounds the flux rope (see illustration in Lin and Forbes, 2000). In the breakout (Antiochos, DeVore, and Klimchuk, 1999) or shearing arcade models (Mikic and Linker, 1994), reconnection may be the cause of the initial instability and may eventually lead to the formation of a flux rope.

Whereas the mass and kinetic energy losses of CMEs are insignificant in the corona, they are considered to play a significant role in removing magnetic flux and helicity that would otherwise build up in the corona. How this may work essentially boils down to the nature of the CME-streamer interaction, *i.e.*, as to whether CMEs respond passively or contribute dynamically to the coronal field restructuring (Liu, 2009). In the view of Low (1996, 1997, 2001), CMEs act as a basic mechanism of coronal magnetic field reconfiguration, removing the old magnetic flux and helicity from the corona to make room for the flux of the new cycle. This requires that a significant number of CMEs induces permanent changes to the coronal field configuration, a process illustrated for example by the artificial introduction of a bipolar active region into the background field (Luhmann *et al.*, 2003). The opposite view has been presented that the global coronal field organization does not respond in a lasting way to CMEs (Sime, 1989) with the streamer belt capable of re-forming itself on a timescale of about two days (Zhao and Hoeksema, 1996). Based on the available analysis summarized above, it is entirely possible that both situations co-exist depending for instance on the pre-CME configuration of the streamer and on the strength of the CME.

An additional aspect which adds to the complexity of the interaction lies in its ambivalence: whereas cases of CMEs breaking up streamers are well documented, the opposite situation where CMEs are deflected by the streamer belt has been noticed as early as the *Skylab* and SMM era (MacQueen, Hundhausen, and Conover, 1986) and has been addressed in numerous articles; see the recent work of Zuccarello *et al.* (2012) for a summary.

The objective of this present work is to perform a systematic study of the CME-streamer interaction over 15 years (1996 to 2010 inclusive), which is more than a solar cycle. Following the introduction, we present our general approach in Section 2. We first describe the synoptic maps of the radiance of the K-corona constructed from a time series of LASCO-C2 images. We then summarize our method of automatic detection of CMEs which led to the creation of the ARTEMIS-II catalog (Floyd *et al.*, 2013) and explain how we perform an automatic characterization of the streamers. An example of the complexity of the CME-streamer interaction based on events observed in December 2007 – January 2008 is discussed in Section 3. Section 4 is devoted to the classification of the interactions and Section 5 presents our statistical results. We conclude in Section 6.

2. General Approach

Our approach follows that pioneered by Hundhausen (1993) in using synoptic maps constructed from SMM data to visualize the general structure of the corona and thus to conspicuously display the belt of coronal helmet streamers as well as additional secondary structures presumably associated with other regions of closed magnetic field lines. His maps display the brightness of the corona, a terminology which is not very clear, and have a longitudinal resolution of $\approx 7°$ (12 h) per pixel and probably the same latitudinal resolution although this is not specified. Nevertheless, they led him to identify "bugles", each one representing the brightening and swelling of the belt for several days before the occurrence of a CME ejection followed by the abrupt disappearance of the streamer after the event and consequently, to start characterizing the CME-streamer relationship on a statistical basis. In his procedure, Hundhausen used the original SMM images to determine the parameters of the CMEs

which were then manually inserted on the synoptic maps as dashed vertical segments at the appropriate longitude and with the observed latitudinal extent. Subramanian *et al.* (1999) essentially implemented the same procedure to the LASCO-C2 data. Their synoptic maps display the ratio of the observed signal to a background model to account for scattered light and the dust (F) corona. They have a longitudinal resolution of 1° (1.82 h) per pixel up to Carrington rotation (CR) 1919 (February 1997) and 0.5° (0.91 h) per pixel thereafter, the latitudinal resolution being 1° per pixel in all cases. Llebaria *et al.* (2006) introduced a novel approach consisting in detecting and characterizing the CMEs directly from the synoptic maps of the radiance of the K-corona constructed from the LASCO-C2 images. This was made possible by the longitudinal and latitudinal resolutions of, respectively, 0.25° (27 min) and 0.5° per pixel of their maps. Whereas the detection of CMEs was fully automated (see also Boursier *et al.*, 2006, 2009 for technical details), their interaction with the streamers was characterized visually over 26 Carrington rotations.

   Our present objective to perform a systematic study of the CME-streamer interaction over 15 years (1996 to 2010 inclusive) required an extra effort to automate the characterization of the streamers and, altogether with the CMEs, the overall procedure.

2.1. The LASCO Synoptic Maps

Synoptic maps of the K-corona radiance corresponding to successive Carrington rotations were constructed from a time series of LASCO-C2 images (≥ 50 per day) first corrected for instrumental effects, and calibrated in units of mean solar radiance. The extensive correction of the raw images, the separation of the K-corona, and the generation of the synoptic maps have been described by Saez *et al.* (2007), Boursier *et al.* (2009), and Floyd *et al.* (2013). The synoptic maps produced by the LASCO team at Laboratoire d'Astrophysique de Marseille as first introduced by Lamy, Llebaria, and Quemerais (2002) are non-standard as they simultaneously display both east and west limbs. Their horizontal or *x*-axis represents time running from left to right (it is equivalent to the longitude of the central meridian of the Sun), and the vertical or *y*-axis represents the solar polar angle running from 0° to 360° starting from the south pole and increasing counterclockwise (instead of the latitude running from $-90°$ to $90°$ in the standard synoptic maps). These non-standard synoptic maps are constructed from K-corona images resized to a common format of 512×512 pixels with two different angular steps: 0.4° for radial distances of 3 and 3.5 $R_\odot$ and 0.25° beyond. A uniform linear resampling with a time step of 27.3 days/1440 = 27.3 min is applied, comparable to the average temporal cadence of the C2 images taken during the last 12 years, that is, ≈ 24 min. These maps have therefore a format of 1440×900 pixels at radial distances of 3 and 3.5 $R_\odot$ and of 1440×1440 pixels at larger distances. Only those obtained at 3 $R_\odot$ were used in the present study, as they offer the best contrast for both the CMEs and the streamers; see Figure 1 for examples.

2.2. Characterization of the Coronal Mass Ejections

The characterization of the CMEs results from their automated detection and the creation of the ARTEMIS databases as described by Boursier *et al.* (2009) for ARTEMIS I and Floyd *et al.* (2013) for ARTEMIS II. In summary, the procedure consists of four steps: filtering, thresholding, segmenting and merging with high level knowledge.

- The filtering consists in subtracting a background K-corona obtained by applying a median filter to the original map with a horizontal window of 6 h.
- The thresholding isolates the most significant structures and returns a 2D binary mask.
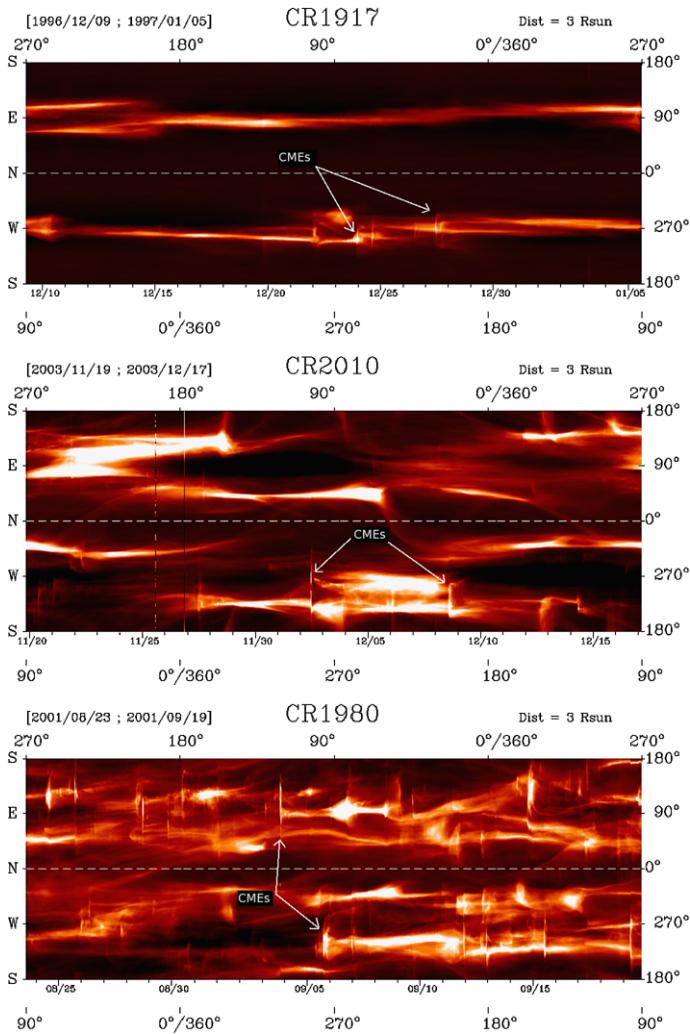
Figure 1 Three examples of LASCO-C2 high definition synoptic maps produced at Laboratoire d'Astrophysique de Marseille for periods of low (top panel), intermediate (middle panel), and high (bottom panel) levels of solar activity. The angles written above and below each synoptic map are respectively the longitudes of the east and west limbs at a given time indicated on the *x*-axis. The arrows point to a few coronal mass ejections conspicuously visible as vertical streaks superimposed on the streamer belt and other coronal structures.

- The segmentation performs a morphological closure to eliminate artificial "holes"; it identifies and labels regions of interests (ROI) with a list of parameters associated with each ROI such as its geometric center and its area.
- The merging with high level knowledge regroups disjoint ROIs if they appear to belong to the same CME based on several conditions, mainly time simultaneity. A mask is finally produced where every CME is represented by a vertical segment whose center is that of the final ROI, and whose vertical extent is its height. Only CMEs with an angular extent

exceeding 7° are kept. Masks obtained at different radial distances are used to determine the velocities.

The ARTEMIS II catalog reports the detection of 21 394 CMEs over an interval of 15 years from 1996 to 2010 and lists their date and time of appearance, position angle, apparent angular width, and intensity. For 58 % of them which were detected at several solar distances ($\approx 13\,000$ CMEs), the catalog further gives their global and median velocities, mass, and kinetic energy.

2.3. Characterization of the Streamers

Classically, the streamer belt appears as bright, more-or-less continuous horizontal bands on synoptic maps. During periods of low solar activity, these bands are almost flat and clearly separate the widespread coronal holes of opposite polarity in the northern and southern hemispheres of the Sun. As activity increases, this simple configuration becomes more and more complex, these bands are distorted by the migration of the solar magnetic field, and many new structures appear. For the purpose of the present study, we consider that streamers are prominently one-dimensional objects, manifesting the boundary between regions of opposite magnetic polarities that can be represented by the line of maximum radiance along them. As such, streamers are defined as ridges on the synoptic maps and an efficient way to detect these ridges consists in applying a watershed filter (Dougherty, 1992). The basic idea behind this filter is to define different regions at each local minimum, and extend these regions by including the adjacent pixels whose values are under a progressively higher threshold. This defines boundaries that progressively extend until those of two regions come into contact, in which case the regions stop extending transversely to these boundaries. Once every pixel in the image belongs to a given region, the boundaries describe all the ridges in the image. The main advantage of the watershed filter over local methods like a differential filter followed by thresholding is that the latter does not properly work near CMEs (the regions we are most interested in) and frequently returns interrupted lines in those regions. Given correct parameters, this problem does not occur with the watershed filter and the ridges are correctly defined right to the vertical discontinuities corresponding to CMEs.

In practice, we applied the filter to sub-images associated with each CME: each sub-image extends longitudinally on both sides of the CME of interest by approximately two days and has the same latitudinal extent as the CME. In addition, the two sides were separately processed so as to decouple the two determinations of the ridge before and after the CME. Once applied, the filter returns the coordinates of the ridges which are then overplotted on the synoptic maps as white lines for a visual check.

2.4. Parameters Characterizing the Interactions

For each CME listed in the ARTEMIS II catalog, we determined several parameters in order to characterize its interaction with the streamers in addition to those present in the catalog, and wrote them in a structure. The scalar fields which characterize the whole CME are:

- the ARTEMIS parameters (position, angular width, velocity, intensity, mass),
- the radiance integrated over the width of the CME,
- the number of streamers on each side

and the vectorial fields which characterize each individual streamer are:

- its peak radiance,
- its total radiance integrated over its latitudinal extent,
- its central position.

2.5. Limitations of the Method

The limitations of the method are essentially those associated with the use of white light images and synoptic maps. The radiance of the corona at a given coordinate in a coronal image is the integral of the light scattered by electrons along the line-of-sight passing through the corona at that coordinate. The integration is particularly important for the streamer belt since it extends quasi-continuously around the Sun and is further pronounced during the minimum of activity when it gets quite flat. However, the integral is usually dominated by contributions from the region where the line-of-sight is closest to the Sun (that is, closest to the plane of the sky) because both the intensity of photospheric radiation and the density of scattering electrons are highest in that region thus partly alleviating the above limitation.

The characterization of both the CMEs and the streamers are based on automatic processes which have their inherent limitations. Regarding CMEs, thresholding has been found to be by far the most critical step in the process of detecting CMEs, and Boursier *et al.* (2009) have thoroughly investigated this question and validated their choice allowing detecting faint events which are not artifacts. The excellent agreement between the CME catalogs based on totally different methods of automatic detection emphasized by Boursier *et al.* (2009) is further a key argument in ascertaining the validity of the detections. Regarding the streamers, the watershed filter will always correctly detect the ridges so the question translates to whether those ridges correctly represent the streamers. To a large extent, this problem is alleviated by the fact that we apply the filter locally to sub-images associated with each CME and separately to the two sides before and after the CME as described in the above section. The very large number of CMEs and of interactions considered in our analysis finally minimizes the impact of possible artifacts in the statistical results.

In the absence of three-dimensional reconstruction of the geometry of the CMEs, their longitude is taken to be that of the east or west limb at the time of observation. In other words, any longitudinal displacement from the plane of the sky is neglected. Likewise, the measured latitude of CMEs is the apparent or projected latitude which is an upper limit of the true latitude because of the fore-shortening effect.

Halo CMEs which usually originate around 90° from the limb and which have very large latitudinal extents cannot be safely associated with streamer configurations observed at the limbs and were therefore excluded from our analysis. Although the CDAW catalog (http://cdaw.gsfc.nasa.gov/CME_list/) sets a lower limit of 270° for the latitudinal extent of halo CMEs, we decided to apply a stricter limit of 180°. This removed 152 CMEs from our initial list bringing the total number of useful events to 21 242.

As alluded in the introduction, the interaction between CMEs and the streamers can be quite complex with CMEs deviating the belt and the belt deflecting CMEs so that a different picture may appear at different distances from the Sun. As coronal helmet streamers "neck down" to a narrow band at distances beyond $\approx 2.5 \ R_\odot$, this sets a lower limit to secure a clear pattern of the belt consistent with the inner field of view of LASCO-C2. Based on SMM images, Hundhausen (1993) observed that the effect of CMEs on the streamers was even more conspicuously apparent at slightly larger distances but this is progressively counterbalanced by the expansion (and therefore dimming) of the CMEs. We therefore adopted a distance of 3 $R_\odot$ as a compromise between the above effects.

3. Complexity of the CME-Streamer Interactions: The December 2007 – January 2008 Events

We selected the December 2007 – January 2008 period to illustrate the complexity of the CME-streamer interactions for several reasons.

- It took place during the minimum phase of cycle 24 so that the streamer configuration is expected to be very simple (Figure 2).
- Two CMEs occurred during that period separated by about 2.5 days.
- It resulted in a diversity of CME-streamer interactions which shows various processes at work.
- The first CME and its impact on the restructuring of the coronal field have been thoroughly studied by Liu (2009) on the basis of STEREO observations and a potential-field source-surface (PFSS) model so that their description of the interaction may be confronted with that given by the LASCO synoptic maps.

Before the occurrence of the first CME of Carrington rotation (CR) 2065 (31 December 2007), the eastern side of the corona between longitudes 200° and 270° was characterized by

 i) a classical helmet streamer slightly south of the equator at latitudes $110-120°$ which roughly coincided with the source-surface neutral line projected onto the synoptic map and

ii) an additional fainter structure at a latitude of $\approx 65°$ described by Liu (2009) as a pseudostreamer separating open field lines of the same polarity, a configuration resulting from the presence of two underlying adjacent loop arcades thus creating a plasma sheet.
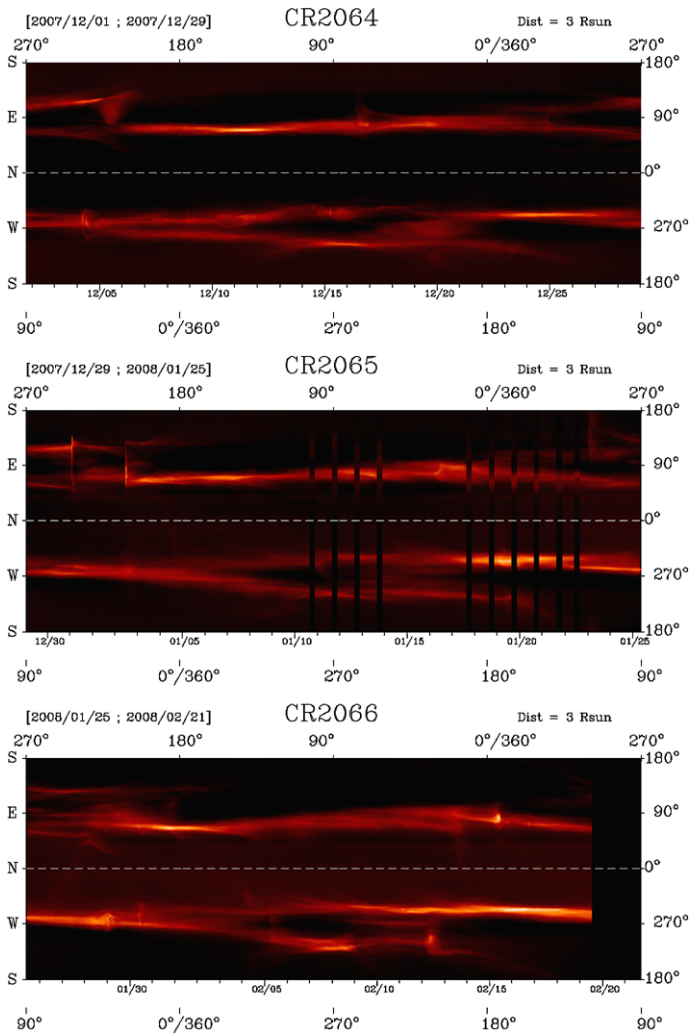
According to the previous synoptic map (CR2064), this pseudostreamer may have evolved from the main streamer belt.

The first CME of 31 December 2007 which originated from NOAA AR 10 978 (Carrington longitude 225° and latitude $-9°$) had two distinct effects. It deflected the helmet streamer to the south and reduced its brightness although a complete blowout did not occur. In a matter of a few hours, the left-over streamer relaxed to its original latitude although fainter than the pre-event streamer. Turning now to the pseudostreamer, the CME likewise displaced it to the south; it became conspicuously brighter but remained stable at its new latitude (*i.e.*, no relaxation) and later initiated a new helmet streamer. Slightly south of this structure, one can discern an additional streamer-like feature most likely corresponding to the post-CME current sheet identified by Liu (2009).

The second CME of 2 January 2008 further upset the above configuration. The left-over streamer which had been progressively declining was once more deflected to the south; after a brief and modest increase, it disappeared in about 1.5 days signaling the complete collapse of the original helmet streamer, itself part of the pre-event belt associated with the heliospheric plasma sheet (HPS). The newly created structure was, on the contrary, displaced to the north and experienced an impressive increase in brightness. As alluded above, it heralds the start of a new stable belt of helmet streamers consistent with the configuration of the neutral line and therefore associated with the new HPS.

Based on the analysis of the first CME of 31 December 2007 by Liu (2009), we can conclude that the course of events as illustrated in their Figure 1 is fully and accurately reflected by our synoptic map (Figure 2). This CME, as well as the second one of 2 January 2008 further reveals the complexity and the diversity of the CME-streamer interaction, far beyond the simple view of streamer blowout. The synoptic maps further offer a global view and in the present example, reveal that the post-CME configuration described by Liu (2009) only held for a couple of days and was itself extensively modified by the second CME of 2 January 2008. Following the eruption of two CMEs in a matter of 2.5 days, the original helmet streamer collapsed and a new one emerged some 50° north probably seeded by the pre-existing pseudostreamer (although it could be a coincidence).

Figure 2 Synoptic map corresponding to CR2065 showing the CMEs of 31 December 2007 and of 2 January 2008 (middle panel). The top and bottom panels, respectively, correspond to the previous (CR2064) and to the next (CR2066) rotations.

4. Classification of the Interactions

The above example has revealed the complexity and variety of the interactions between CMEs and streamers. The statistical analysis of these interactions for thousands of events over 15 years require that we first identify a limited number of categories so that we can then proceed with an automated classification. This was even necessary for the past visual classifications and we briefly review the two past definitions applied to the LASCO data. Subramanian *et al.* (1999) defined four categories, "creates streamer", "displaced from streamer", "streamer blowout", and "no effect". Llebaria *et al.* (2006) considered five categories, "brightening", "dimming", "deviation", "splitting", and "no change". The visual inspection of a large number of cases on many synoptic maps confirms the perception that

the interactions essentially translate into the emergence and disappearance of streamers, in geometric perturbations (*e.g.*, deviation), and in photometric variations (*e.g.*, brightening); in addition the absence of interaction is also observed. Although these effects are not strictly independent (for example many CMEs induce both a deviation and a photometric variation), we felt that they do correspond to widespread situations legitimating their introduction.

We defined six categories of interactions which we selected for our analysis and which basically blend those of Subramanian *et al.* (1999) and Llebaria *et al.* (2006). The photometric variations led to define two categories, "brightening" and "dimming". The geometric variations led to define three categories, "emergence", "disappearance", and "deviation". The last category "no change" contains all cases where none of the above variations is observed. Comparing pre- and post-CME streamers requires that we assume a one-to-one relation, a condition which raises problems when multiple streamers are involved, typically during periods of maximum solar activity. Let us denote N_b and N_a the numbers of streamers associated with a given CME, respectively, before and after its occurrence, *i.e.* streamers having latitudes comprised in the latitudinal extent (or angular width) of this CME. Whenever $N_b > 1$, identifying the cases of "brightening", "dimming", and "deviation" will be limited to the pre-event streamer whose latitude is closest to that of the center of the related CME; the associated post-event streamer in case $N_a > 1$ will be that one whose latitude is closest to the latitude of the pre-event streamer. Pre- and post-CME streamer radiances and latitudes are recorded 7 h (that is 15 pixels) before and after the time of occurrence of the CME to avoid irrelevant rapid and small-scale variations that sometimes take place very near the time of eruption. The final values are in fact averaged over an interval of 2.5 h (5 pixels) to produce robust determinations. Classifying the interactions in the "emergence" and "disappearance" categories is straightforwardly performed by comparing N_b and N_a. We describe below these categories in detail and give a typical example for each one.
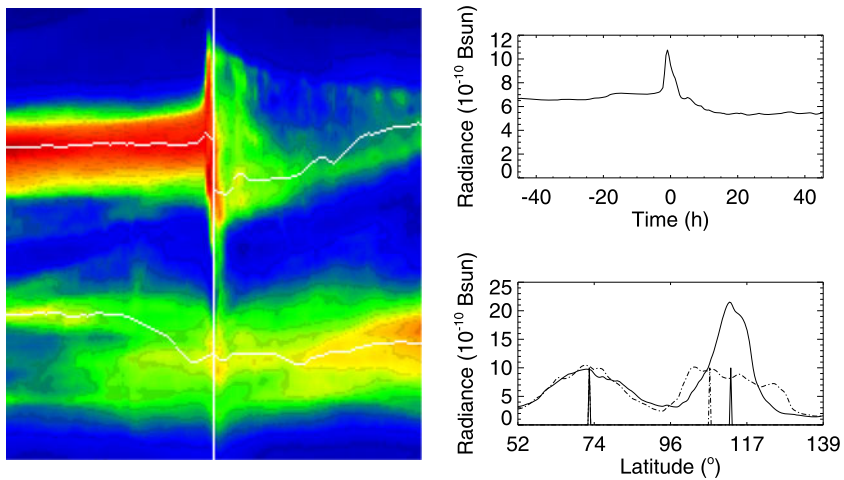
4.1. Dimming

This category contains the cases where a pre-CME streamer suffers a measurable decrease in radiance after the occurrence of the CME. A remarkable example can be seen with CME CR1929_008 of 4 November 1997 in Figure 3. The plot of the radiance indicates a reduction by a factor ≈ 2 in a very short time, and the image indicates that the dimming of the post-CME streamer persisted for a few hours. Note that the other streamer crossed by the CME is photometrically unaffected though, apart from a slight and very brief angular deviation.

Table 1 reports some other remarkable events and displays the dimming ratio which ranges from 0.36 to 0.89 in those cases. Substantial decreases by factors exceeding two are observed and those extreme interactions may be assimilated to streamer blowouts (Howard *et al.*, 1985).

4.2. Brightening

This category contains the cases where a pre-CME streamer experiences a measurable increase in radiance after the occurrence of the CME. An example of a brightening taking place in a quiet corona is visible in Figure 4 associated with CME CR1934_046 of 27 March 1998. The increase in radiance amounts to a factor ≈ 1.4 and progressively decreases after the event until a second CME occurs.

Table 1 reports a few other remarkable events and lists the brightening ratio which ranges from 1.2 to 2.5 in those cases.

Figure 3 Example of streamer dimming following the occurrence of CME CR1929_008 of 4 November 1997. The image centered at the CME extends over a total time interval of 3.8 days (50°) and over the same angular width as the CME (86°). The upper right panel displays the temporal (*i.e.*, longitudinal) evolution of the radiance integrated over the latitudinal range of the upper streamer which underwent a significant dimming. The lower right panel displays the latitudinal radiance profiles across the streamers extracted 8 h before (solid line) and after (dashed-dotted line) the CME. The estimated position of the streamers at these times is indicated by vertical segments of the same type on the lower right panel.

4.3. Emergence and Disappearance

These two categories simply contains the cases where N_b and N_a, the numbers of pre- and post-streamers associated with a given CME, are different from obvious emergence corresponding to $N_a > N_b$ and disappearance to $N_a < N_b$. Examples of emergence and disappearance are displayed in Figure 5.

4.4. Deviation

This category contains the cases where there is a measurable difference between the latitudes of the pre- and post-CME streamers subject to the conditions imposed in the introduction of this section. An example is displayed in Figure 6 where CME CR1931_033 of 11 January 1998 deviates the pre-existing streamer by approximatively 10° in a few hours and the displaced post-event streamer remains at about the same latitude for more than a day. It appears a bit narrower than the original streamer but the (vertically) integrated radiance profiles remains fairly constant. Note that, in this particular case, a new slightly brighter streamer appears thereafter, somehow reminiscent of the pre-event streamer. We noticed that deviations are mostly of two kinds:

 i) temporary deviations, of small amplitudes, with the post-event streamer going back to the pre-event latitude in a few hours and
ii) permanent deviations with the post-event streamers remaining stable at its next location for many days.

Table 2 reports other cases of angular deviation which range from 4 to 21°.
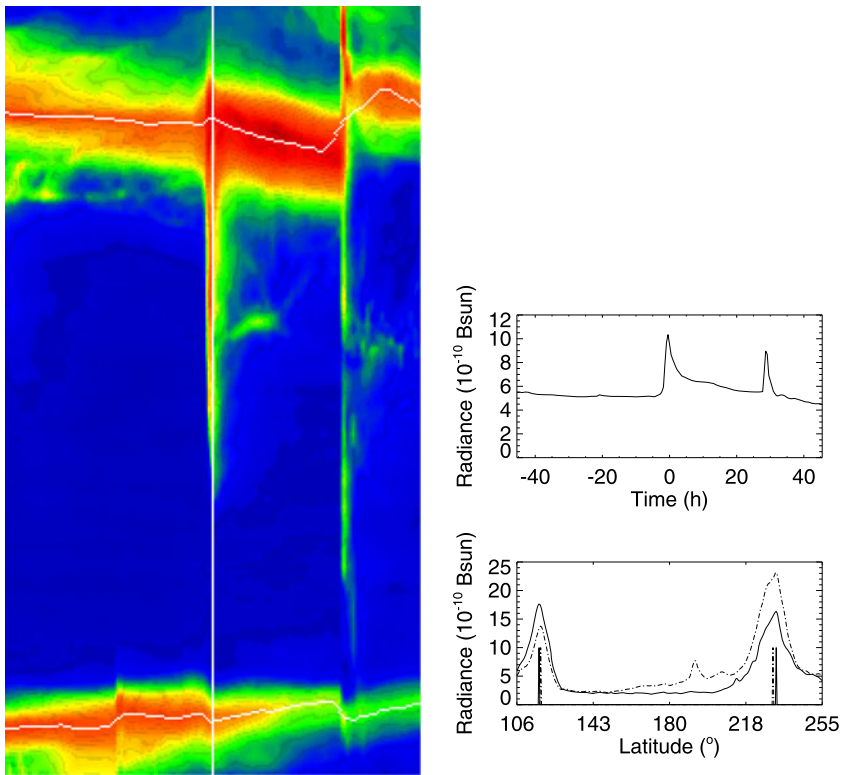
Figure 4 Example of streamer brightening following the occurrence of CME CR1934_046 of 27 March 1998. The image is centered at the CME and extends over the same angular width (149°). See further explanations of the accompanying graphs in the caption to Figure 3.

4.5. No Change

This category contains cases which, unlike those of the previous categories, have no significant effect on the streamer, either photometric or geometric. An example is displayed in Figure 7 with CME CR1953_174 of 7 September 1999. The average radiance of the streamer keeps slightly increasing at a regular rate irrespective of the CME occurrence and the streamer only shifts by less than 3° for just a few hours. Note that this CME with a mass of 3.2×10^{15} g belongs to the 10 % brightest CMEs of the ARTEMIS II catalog implying that it is a significant event which could have disrupted the streamer.

5. Statistical Results for the CME–Streamers Interactions

Having characterized the CMEs and streamers on the synoptic maps and defined the categories of interaction, we are now in position to proceed with the statistical analysis of the interactions for the whole set of CMEs detected on the LASCO-C2 synoptic maps from 1996 to 2010, excluding the halo events as explained in Section 2.5; this will be thereafter denoted the "global set" of CMEs. By extension, we will apply the same terminology when considering a category of CMEs, implying that we are considering all CMEs of this category. The

Table 1 Properties of a few cases of dimming (upper part) and brightening (lower part).

CME ID	AW (°)	Pre-CME radiance (10^{-10} $B_\odot$)	Post-CME radiance (10^{-10} $B_\odot$)	Ratio
CR1929_008	86	21	10	0.47
CR1930_006	81	17	15	0.89
CR1934_033	70	29	17	0.59
CR1936_083	86	19	15	0.81
CR1936_105	71	28	11	0.39
CR1970_033	158	26	10	0.41
CR1980_177	37	30	16	0.55
CR1985_071	110	34	12	0.36
CR2002_114	54	47	27	0.59
CR2003_173	55	28	14	0.50
CR1919_012	90	13	17	1.31
CR1934_046	149	16	23	1.42
CR1966_197	119	19	23	1.19
CR1973_008	117	10	17	1.71
CR1988_109	40	15	38	2.51
CR1996_019	61	22	29	1.32

Note:
    CME ID: identification in the ARTEMIS II catalog.
    AW: apparent angular width of the CME.
    Ratio: ratio of the radiances of the post- and pre-CME streamers.

Table 2 Properties of a few cases of deviation.

| CME ID	AW (°)	Pre-CME radiance (10^{-10} $B_\odot$)	Post-CME radiance (10^{-10} $B_\odot$)	Deviation (°)
CR1931_033	75	15	12	8.4
CR1935_050	134	15	16	19.2
CR1954_023	125	19	11	16.0
CR1965_097	121	20	22	8.4
CR1966_197	119	20	15	4.4
CR1986_188	141	30	38	6.4
CR1992_037	136	16	21	6.8
CR1995_052	144	27	33	20.8

Note:
    CME ID: identification in the ARTEMIS II catalog.
   AW: apparent angular width of the CME.
    Deviation: angular distance between the post- and pre-CME streamers.

automated detection of CMEs on the high quality LASCO-C2 images has led to the iden-
tification of a large population of faint transients which may simply be travelling "blobs"
comprising the slow solar wind so that their assimilation to "true" CMEs raises questions
(Boursier *et al.*, 2009; Robbrecht, Berghmans, and Van der Linden, 2009). In order to assess
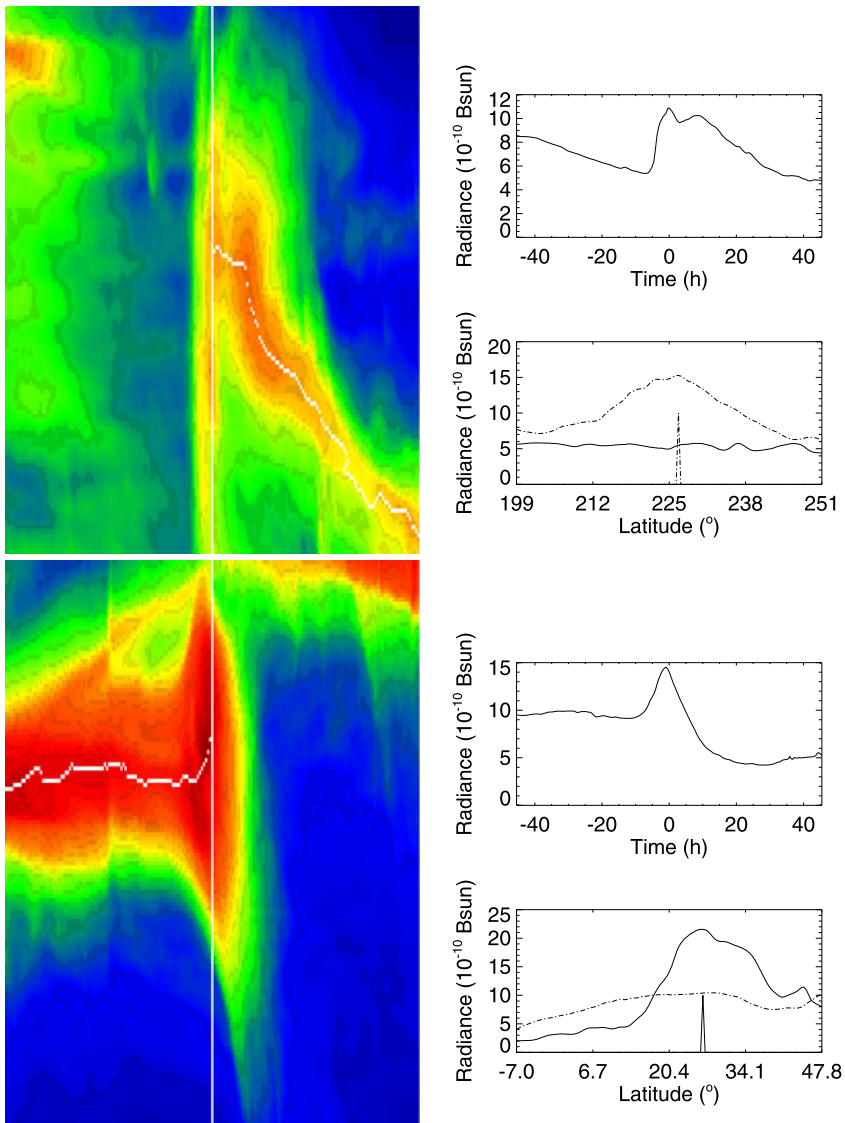
Figure 5 Examples of a case of emergence (top image) and of disappearance (bottom image) for CMEs CR1997_135 of 24 December 2002 and CR1977_146 of 16 June 2001. Each image is centered at the CME, and their latitude extends over 77°. See further explanations of the accompanying graphs in the caption to Figure 3.

a possible bias resulting from that population, we systematically performed a parallel analysis on the restricted subset of the 10 % brightest CMEs using the intensity parameter of the ARTEMIS II catalog. For simplicity, this subset will be denoted "top-ten" CMEs thereafter. Here again, we will apply the same terminology when considering a category of CMEs, implying that we are considering the subset of the 10 % brightest CMEs that belongs to this category. We will further distinguish three typical periods of solar activity defined by the
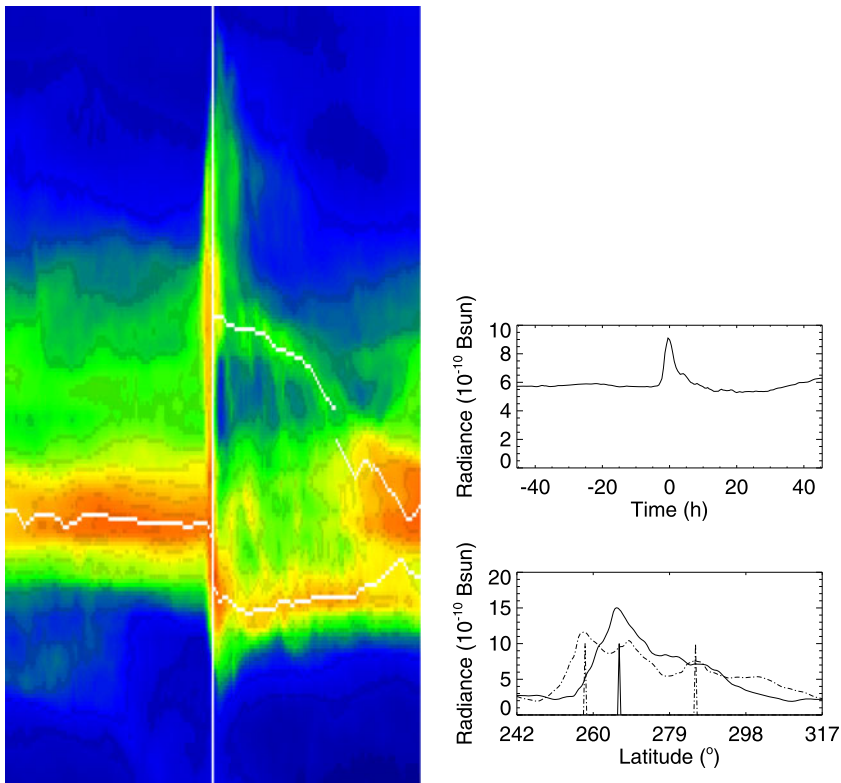
Figure 6 Example of a case of deviation following the occurrence of CME CR1931_033 of 11 January 1998. The image is centered at the CME and extends over 75°. See further explanations of the accompanying graphs in the caption to Figure 3.

following Carrington rotations: CR1910 to CR1930 (June 1996 – December 1997) for minimum activity, CR2000 to CR2020 (March 2003 – September 2004) for intermediate activity, and CR1970 to CR1990 (December 2000 – June 2002) for maximum activity.

5.1. Statistical Results for the CME-Streamers Association

We first address the very question of the association between CMEs and streamers. This is part of a broader investigation where we counted the number of pre- and post-CME streamers, respectively (N_b and N_a, to be discussed in detail in the next section). A CME-streamer association does not exist whenever no streamer either before or after the CME has its latitude comprised in the latitudinal extent (or angular width) of the considered CME. In terms of counting the number of pre- and post-CME streamers, this obviously corresponds to the case $N_b = N_a = 0$ denoted $C(0, 0)$ and the corresponding results are shown in Tables 3 and 4.

A striking outcome is that 47 % of the global set of CMEs are not associated with any streamer, either before or after the event; however, this percentage drops to 7 % when considering the "top-ten" CMEs. This trend is readily understood when comparing the intensity distributions of the two subsets of CMEs, respectively, belonging to cases $C(0, 0)$ and $C(N_b \geq 1, \ N_a \geq 1)$ in Figure 8: the first one is skewed by faint CMEs with a peak at $\approx 10^2$
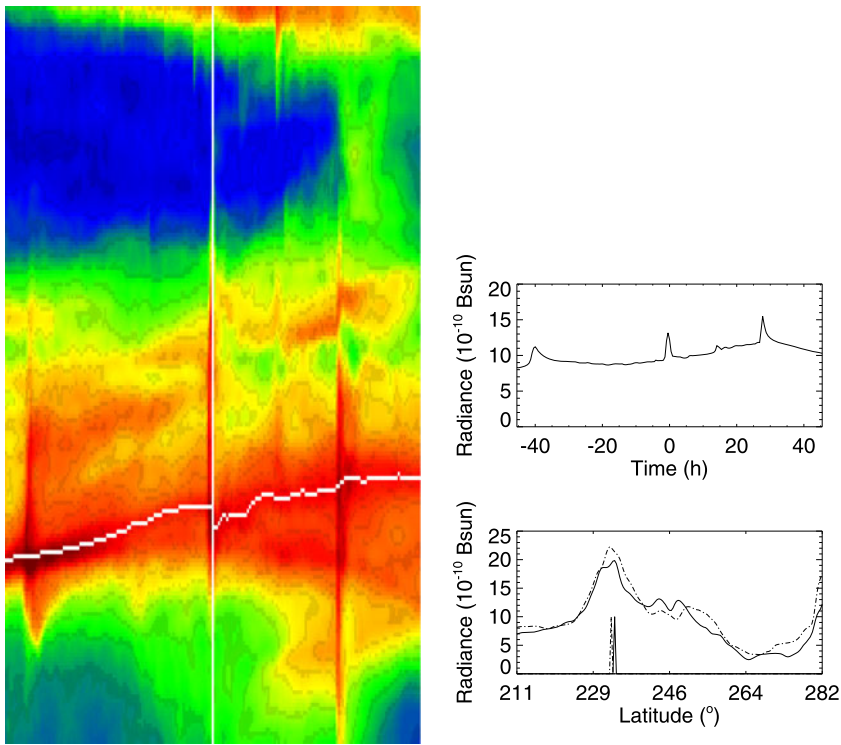
Figure 7 Example of a CME (CR1953_174 of 7 September 1999) having no significant effect on the streamer. The image is centered at the CME and extends over the same angular range as the CME (71°). See further explanations of the accompanying graphs in the caption to Figure 3.

Table 3 Distribution of the number of CMEs of the global set belonging to cases $C(N_b, N_a)$ where N_b and N_a are the numbers of streamers, respectively, before and after the occurrence of a CME. The results are displayed in percentages and in number of CMEs in parentheses.

N_a	N_b			
	0	1	2	3
0	47.3 % (8617)	11.0 % (1994)	0.9 % (161)	0.1 % (22)
1	10.1 % (1832)	16.9 % (3081)	3.4 % (625)	0.5 % (93)
2	0.8 % (152)	3.5 % (629)	2.9 % (529)	0.8 % (142)
3	0.1 % (22)	0.5 % (100)	0.8 % (137)	0.4 % (71)

Total = 18207 CMEs

whereas the second one is more symmetric with a peak at $\approx 10^3$, both extending over approximately two decades of intensity. Clearly, the bulk of the faint CMEs are not associated with any streamers unlike the "top-ten" CMEs. As will be further elaborated in the next section, the percentages of CMEs not associated with any streamer do not vary significantly with solar activity.

Table 4 Distribution of the number of CMEs of the "top-ten" subset belonging to cases C(N_b, N_a). See Table 3 for explanations.

N_a	N_b			
	0	1	2	3
0	7.0 % (123)	8.4 % (147)	1.5 % (27)	0.3 % (5)
1	4.2 % (73)	27.2 % (479)	10.9 % (192)	2.3 % (40)
2	0.9 % (16)	10.9 % (192)	12.8 % (225)	4.5 % (79)
3	0.2 % (4)	2.0 % (35)	4.5 % (79)	2.4 % (42)

Total = 1758 CMEs

Figure 8 Intensity distributions of the two subsets of CMEs, respectively, belonging to cases $C(0, 0)$ (solid line) and $C(N_b \geq 1,\ N_a \geq 1)$ (dash-dotted line).
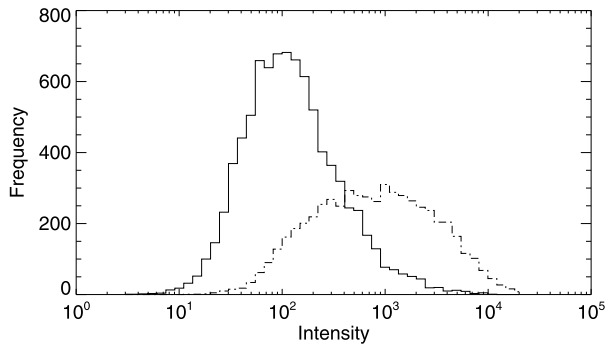
We next calculated for each CME which has an associated pre-CME streamer the angular distance between the latitude of its center and that of the axis (*i.e.*, the ridge) of the nearest pre-CME streamer. The distances were so calculated that deviations towards the equator are positive and away from it negative with the purpose of investigating whether there is any distinct trend with solar activity. Figure 9 displays the distributions of distances for the global set and the "top-ten" CMEs satisfying the above conditions. Both distributions are centered at 0° and nearly symmetric, that of the "top-ten" CMEs being slightly broader. Those are remarkable results in view of the inherent difficulties associated with the automatic definition of the center and of the axis of such diverse and ill-defined objects as CMEs and streamers. In fact, the width of the distributions probably reflects in part the uncertainties associated with the procedure. Similar histograms were generated for the three cases of activity and the results are presented in a synthetic form of cumulative distribution functions (CDFs) as displayed in Figure 10 for the global set only as the results for the "top-ten" CMEs look very similar. For both populations, the distributions are slightly narrower (by 5 to 10°) and slightly skewed to positive distances in the case of minimum activity compared to the two other cases. Therefore, the only emerging and possible trend is for CMEs to move away from their associated streamer towards the equator during the minimum of activity.

5.2. Statistical Results for the Emergence and Disappearance of Streamers

As outlined in the above section, this study was achieved by counting the number of streamers having latitudes comprised in the latitudinal extent (or angular width) of a given CME, before (N_b) and after (N_a) its occurrence. Both N_b and N_a were limited to three as we thought that it would make little physical sense to go beyond. This limitation left aside 3035

Figure 9 Distribution of the streamer-CME angular distance for CMEs having a pre-event streamer: global set (upper panel) and "top-ten" CMEs (lower panel).
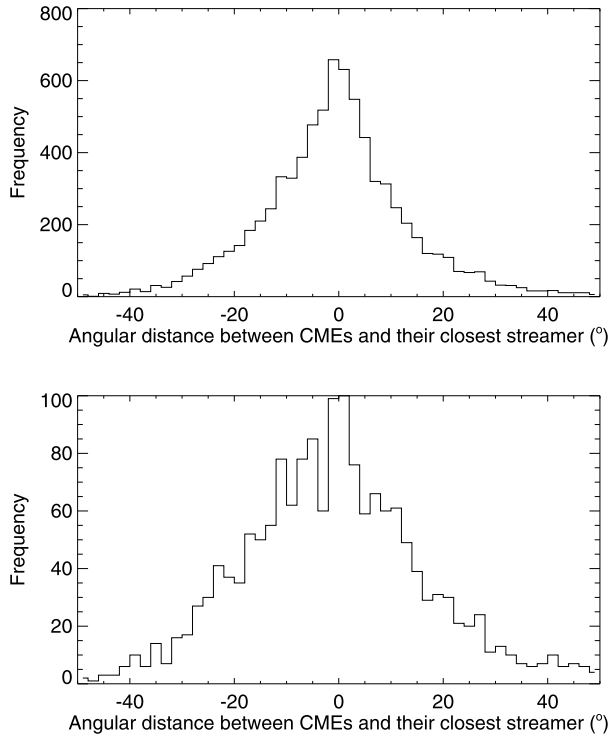
Figure 10 Cumulative distribution functions of the streamer-CME angular distance for the global set of CMEs having a pre-event streamer and for three cases of solar activity.
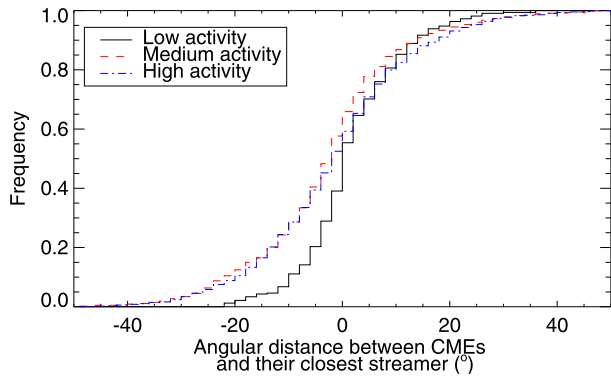
CMEs out of a total of 21 242 in the ARTEMIS II catalog, that is, 14 %. Therefore N_b and N_a take values from 0 to 3 leading to 16 cases that we denote $C(N_b, N_a)$. All results are summarized in Table 3 for the overall 18207 CMEs and in Table 4 for the 1758 "top-ten" CMEs where the numbers of CMEs are given in absolute value (in brackets) and in percent. We note that the cases where $N_b = 3$ or $N_a = 3$ are by far less numerous, *a-posteriori* justifying our limitation.

An approximate symmetry is observed with respect to the $N_b = N_a$ diagonal where the largest numbers are present thus implying that the emergence and the disappearance of streamers are not dominating processes. A closer look reveals that for the "top-ten" CMEs,

the symmetry is in fact systematically skewed to the cases corresponding to $N_b > N_a$ meaning that the emergence of streamers is slightly less frequent than their disappearance. Accumulating all cases corresponding to emergence ($N_b < N_a$) and disappearance ($N_b > N_a$), we found nearly the same percentages (16–17 %) for the global set whereas disappearance (28 %) exceeds emergence (23 %) for the "top-ten" subset.

As already noted, 47 % of the global set of CMEs are not associated with any streamer, either before or after the event; this percentage drops to 7 % when considering the "top-ten" CMEs. Conversely, the other diagonal terms and significantly $C(1, 1)$ and $C(2, 2)$ are much larger for the "top-ten" CMEs than for the global set.

The influence of solar activity on these distributions is graphically illustrated for the seven most significant cases in Figure 11. These three periods include 755 CMEs at the minimum, 2462 at the intermediate and 4440 at the maximum phases in the global sets, and respectively 72, 231, and 485 in the "top-ten" CMEs.

The percentages of CMEs not associated with any streamer, that is, case $C(0, 0)$, remain fairly constant for the two sets of CMEs. This is not the case of the diagonal terms as the percentage of CMEs belonging to $C(1, 1)$ decreases with increasing activity whereas that of CMEs in $C(2, 2)$ follows the inverse evolution, quite pronounced for the "top-ten" CMEs and less so for the global set. The increasing number of streamers as activity develops most likely explains that an increasing number of them is associated with CMEs atop the concurrent increase of the number of CMEs.

Concerning the cases which correspond to the emergence of streamers, the percentages of CMEs belonging to $C(0, 1)$ are systematically larger for the global sets than for the "top-ten" CMEs whereas the opposite situation prevails for the CMEs in $C(1, 2)$; no clear trend with solar activity is observed in both cases.

Concerning the cases which correspond to the disappearance of streamers, the percentages of CMEs belonging to $C(1, 0)$ are systematically larger for the global sets than for the "top-ten" CMEs whereas the opposite situation prevails for the CMEs in $C(2, 1)$. There is, however, one exception corresponding to the $C(1, 0)$ case at intermediate activity for which the percentage of "top-ten" CMEs slightly exceeds that of the global subset (this number was thoroughly checked; it corresponds, however, to only 30 CMEs). The variations with solar activity of the percentages corresponding to the $C(1, 0)$ and $C(2, 1)$ cases for the global subsets remain quite limited whereas they appear more pronounced for the "top-ten" CMEs although no clear trend emerges. Note in particular the absence of consistent evolution from the minimum to the maximum of activity. These results should be viewed with caution as they constitute only small fractions of the overall sets, either global or "top-ten".

5.3. Statistical Results for the Deviations

In order to characterize the statistical properties of the deviations, we systematically calculated the differences in the latitudes of the pre- and post-CME streamers subject to the conditions stated in Section 4, namely that whenever $N_b > 1$, the pre-event streamer is the one whose latitude is closest to that of the center of the related CME and the associated post-event streamer in case $N_a > 1$ is the one whose latitude is closest to the latitude of the pre-event streamer. The distribution of these differences for the global set of CMEs is displayed in Figure 12. It is unimodal, centered at 0°, and symmetric, which means that

 i) the classification in terms of deviation must come from an arbitrary threshold and
ii) there is no preferred direction for the deviations.

The corresponding cumulative distribution functions for the global set and "top-ten" CMEs are displayed in Figure 13. We can see that the distribution in the latter case is slightly
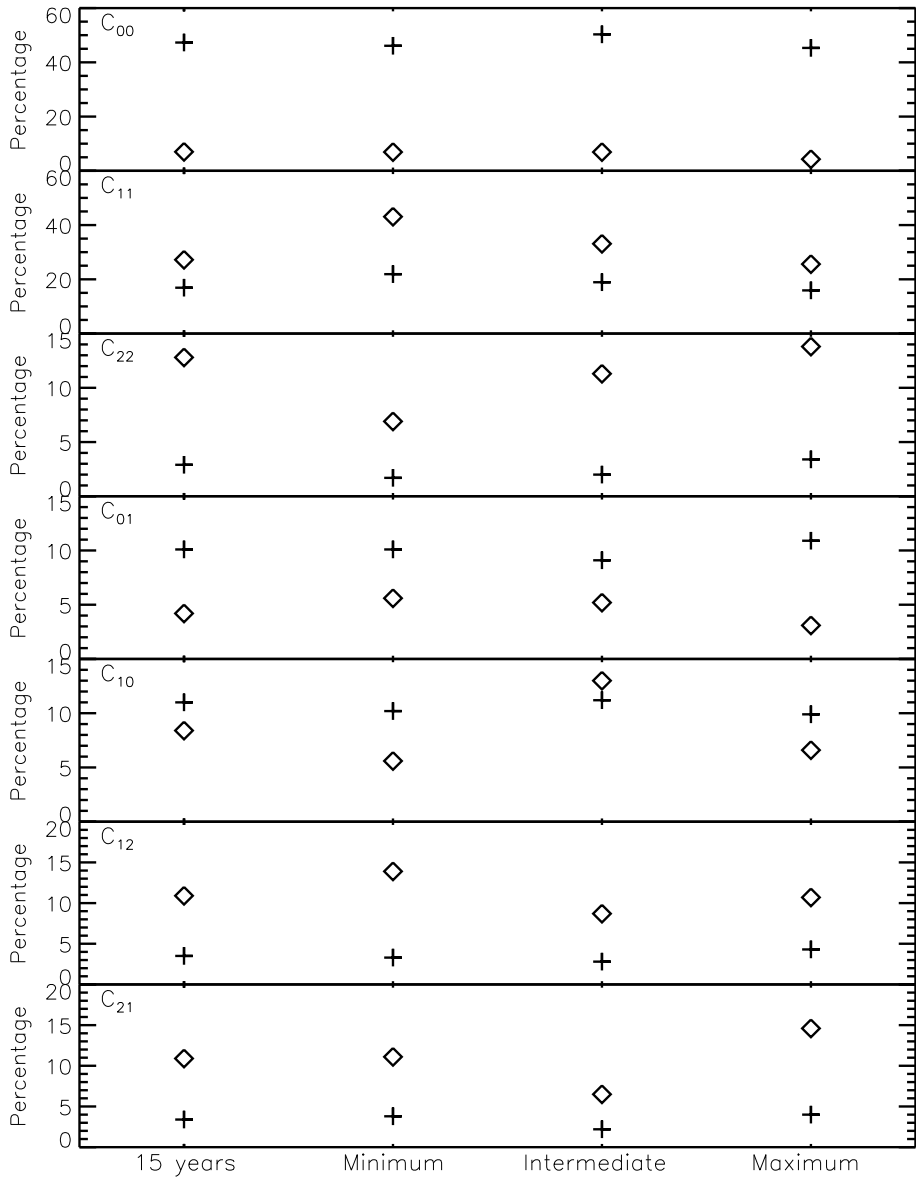
Figure 11 Percentages of CMEs belonging to the seven main cases C($N_b \leq 2$, $N_a \leq 2$). Values are given for the global subsets (plus symbols) and for the "top-ten" subsets (star symbols). The leftmost column of results corresponds to the 15 years of observation as labeled on the x-axis. The other three columns correspond to the three periods of solar activity: minimum, intermediate, and maximum.

broader, but just by $\approx 2°$ and that the deviations rarely exceed $\approx 10°$. Adopting a threshold of $\pm 1.6°$ (4 pixels) to define a significant deviation accounting for the inherent uncertainties in the automatic procedure, we found that 57 % and 70 % of, respectively, the global set and "top-ten" CMEs have their associated streamers undergoing a deviation. Figure 13

Figure 12 Distribution of streamer deviations for the global set of CMEs.
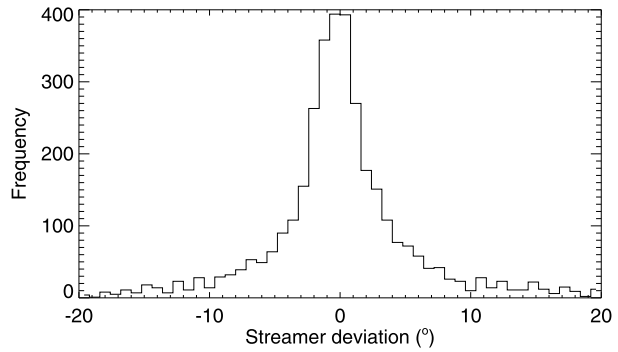
Figure 13 Cumulative distribution functions (CDFs) of the streamer deviation. Upper panel: CDFs for the global and "top-ten" sets. Middle panel: CDFs for the global subsets corresponding to the three periods of activity. Lower panel: CDFs for the "top-ten" subsets corresponding to the three periods of activity.
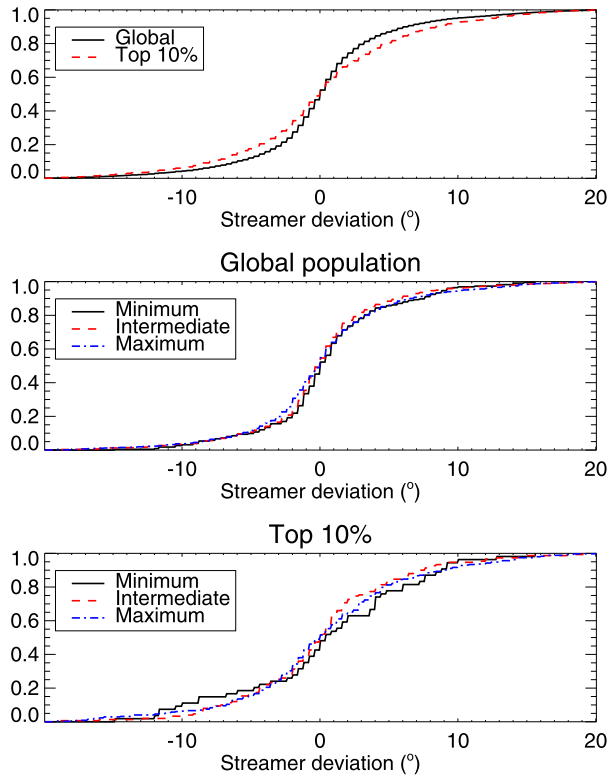

further reveals the lack of any significant influence of solar activity on the deviation process.

5.4. Statistical Results for the Photometric Variations

To study the statistics of the photometric variations, we proceeded likewise the deviations but considered the ratio between the radiances of the pre- and post-CME streamers. Figure 14 displays the distribution of the ratio of radiances for the global set of CMEs. Very much like the category of deviations, it is unimodal, centered at 1, and extends roughly from 0.5 to 1.6. This means that

Figure 14 Distribution of the
ratio of the radiances of the pre-
and post-CME streamers for the
global population of CMEs.
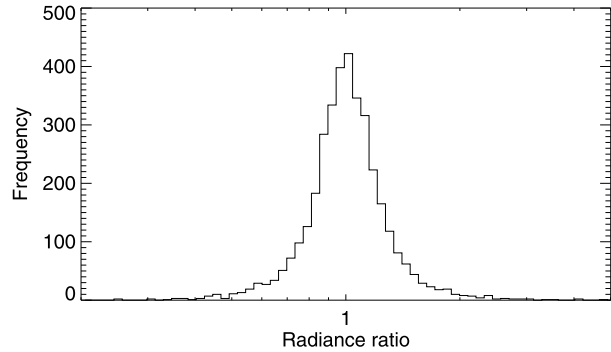
 i) the classification in terms of dimming and brightening must come from an arbitrary
    threshold and
ii) the two types of photometric variation are equally present.

The corresponding cumulative distribution functions of the radiance ratio for the global set
and "top-ten" CMEs are displayed in Figure 15. We can see that the distribution in the latter
set is slightly broader in the case of dimming.

Adopting thresholds of 0.9 and 1.1 to define a significant photometric variation to account
for the inherent uncertainties in the automatic procedure, we found that 29 % and 36 % of
respectively the global set and "top-ten" CMEs have their associated streamers experienc-
ing a dimming, and that 31 % of both sets have their associated streamers experiencing a
brightening.

Figure 15 further shows the lack of any significant influence of solar activity on the
photometric variations.

5.5. Correlation Between the Geometric and Photometric Variations

As already noted, these two types of variations do not define independent categories of
interactions so that we wondered about a possible correlation between them. This question
is considered by analyzing the scatter plots of the ratio of the radiances of the pre- and post-
CME streamers and of the streamer deviation. Figure 16 conspicuously shows that the global
set and the "top-ten" CMEs exhibit similar patterns indicating the absence of correlation.

5.6. Statistical Results for the "No Change" Category

The "no change" category is defined by the condition $N_b = N_a$ and by imposing the thresh-
olds introduced in the above subsections for the deviation (within the interval of $\pm 1.6°$) and
for the photometric variation (within the interval $0.9 - 1.1$). We calculated the percentages
with respect to the global set and the "top-ten" CMEs excluding the cases $C(0, 0)$ which
correspond to the absence of pre- and post-CME streamers and found respectively 6 % and
5 % for the two sets. The results for the three periods of solar activity are reported in Ta-
ble 5. There is not much difference between the global set and the "top-ten" CMEs. The
percentages of "no change" cases increase with activity but surprisingly, the largest values
are observed during the intermediate period. These results are somewhat puzzling, as we in-
tuitively would have expected the opposite situations to prevail with the "no change" events
being more numerous during the period of low activity.

Figure 15 Cumulative distribution functions (CDFs) of the ratio of the radiances of the pre- and post-CME streamers. Upper panel: CDFs for the global and "top-ten" sets. Middle panel: CDFs for the global subsets corresponding to the three periods of activity. Lower panel: CDFs for the "top-ten" subsets corresponding to the three periods of activity.
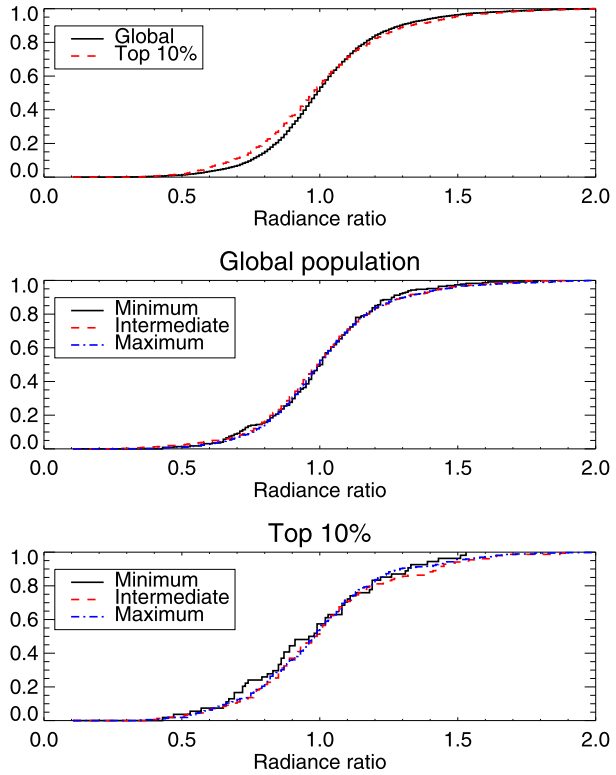
Figure 16 Scatter plots of the ratio of the radiances of the pre- and post-CME streamers and of the streamer deviation. Upper panel: global set of CMEs. Lower panel: "top-ten" CMEs.
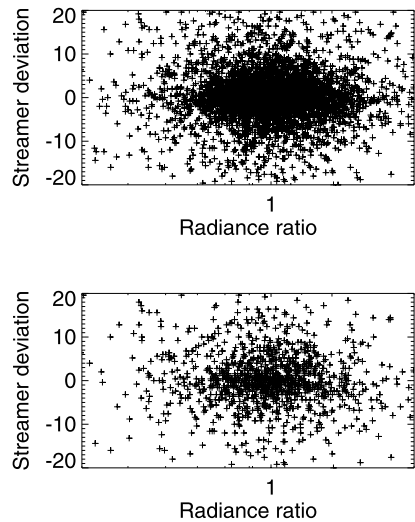
5.7. Influence of the Velocity of CMEs

As mentioned in the introduction, Llebaria *et al.* (2006) noticed that $\approx 50\%$ of the CMEs with velocities exceeding $400\ \mathrm{km\,s^{-1}}$ have no effect on the streamers whereas all slower

Table 5 Statistical results for the "no change" category of CME-Streamer interaction for the global and "top-ten" subsets of CMEs. Upper part: results for the 15 years of observation and for the three periods of activity (minimum, intermediate, and maximum). Lower part: results for two intervals of velocity.

Case	Set	
	Global	Top 10 %
15 years	6 %	5 %
Minimum	2 %	1 %
Intermediate	8 %	7 %
Maximum	5 %	3 %
$V \leq 250 \text{ km s}^{-1}$	7 %	6 %
$V \geq 400 \text{ km s}^{-1}$	6 %	4 %

CMEs affect them one way or the other. We therefore investigated this question on the basis of our much larger data set and calculated the percentages of the "no change" events in two widely separated velocity ranges, namely $V \leq 250 \text{ km s}^{-1}$ and $V \geq 400 \text{ km s}^{-1}$ (we used here the "global" velocity of the ARTEMIS II catalog, see Floyd *et al.*, 2013). These conditions define two roughly identical subsets of CMEs amounting to ≈ 25 % of the original sets of "no change" events. If the conclusion of Llebaria *et al.* (2006) was correct then the above two percentages would amount to ≈ 50 % for the fast CMEs and ≈ 0 % for the slow ones. Our results displayed in Table 5 show that this is not the case as there is no significant difference between the two subsets of slow and fast whether considering the global or "top-ten" CMEs, thus implying no influence of the velocity of CMEs on their interaction with the streamers. Table 5 further shows that the percentages of "no change" in the two widely separated velocity ranges are well in line with those obtained without any constraint on the velocity. We therefore do not confirm the early conclusion of Llebaria *et al.* (2006) which may have been biased by their visual selection of a limited number of events.

6. Conclusions

We have performed a statistical analysis of the interactions between coronal mass ejections and streamers over 15 years from 1996 to 2010 inclusive based on high resolution synoptic maps at 3 $R_{\odot}$ constructed from the whole set of white light images obtained with the LASCO-C2 coronagraph. CMEs and streamers have been automatically detected on the synoptic maps and five categories of interaction have been defined based on photometric and geometric variations between the pre- and post-CME streamers: "brightening", "dimming", "emergence", "disappearance", and "deviation". A sixth category "no change" includes all cases where none of the above variations is observed. The identification of the interactions has dealt with a set of 21 242 CMEs that excludes halo CMES whose latitudinal amplitude exceeds 180° (denoted "global set"). We have considered a subset of the 10 % brightest CMEs (denoted "top-ten") and three typical periods of solar activity: minimum, intermediate, and maximum. The main conclusions of our analysis are summarized below.

  i) About half (precisely 47 %) of the global population of CMEs are not associated with streamers whereas 93 % of the 10 % brightest CMEs are.
 ii) The distributions of the streamer-CME angular distance for those CMEs having a pre-event streamer are remarkably peaked at 0° and symmetric for the two sets, global and "top-ten". A slight skewness is, however, observed during the minimum of activity suggesting a possible trend for CMEs to move away from their associated streamer towards the equator.

iii) When there is a CME-streamer association, approximately 95 % of the streamers experience a change, either geometric or radiometric. Converserly, the "no change" category amounts to approximately 5 %, irrespective of the set considered, global or "top-ten", and irrespective of the CME velocity. This percentage varies from $1 - 2$ % during minimum to $7 - 8$ % during intermediate periods of activity; intermediate values of $3 - 5$ % are recorded during maximum.

iv) Emergences and disappearances of streamers are not dominating processes. Altogether, they constitute $16 - 17$ % of the global set and 23 % (emergence) and 28 % (disappearance) of the "top-ten"set but the individual cases $C(N_b < N_a)$ and $C(N_b > N_a)$ exhibit diverse behaviors. Variations of these percentages with solar activity remains quite limited but more pronounced for the "top-ten" CMEs.

v) Streamer deviations are observed for 57 % and 70 % of respectively the global set and "top-ten" CMEs. The distributions of deviation are symmetric, remain limited to $\approx 10°$, and are influenced by solar activity.

vi) The cases of dimming and brightening are roughly equally present and each case constitutes approximately $30 - 35$ % of either set, global and "top-ten". No influence of solar activity is noted.

To be fully understood and meaningfully compared to past analysis, our results need to be placed in the context of the superior performances of the LASCO-C2 coronagraph and those of the automatic algorithms to detect CMEs. Both concur to detect a record number of CMEs with a substantial fraction of faint transients which went unnoticed in the pre-SOHO era. As already pointed out, these latter events may simply be travelling "blobs" so that their assimilation to "true" CMEs raises questions (Boursier *et al.*, 2009; Robbrecht, Berghmans, and Van der Linden, 2009). This situation was behind our decision to consider the subset of the 10 % brightest CMEs as more representative of their traditional (visual) perception.

Neither Hundhausen (1993) nor Subramanian *et al.* (1999) have isolated a population of CMEs that are not associated with any streamer whereas we found that this situation prevails for a large fraction (47 %) of our global set of CMEs; this fraction, however, drops to only 7 % when considering the "top-ten" CMEs implying that the bulk of the bright CMEs are indeed associated with a pre-existing streamer. To avoid a possible confusion here, we stressed that the "unrelated to pre-existing streamer" set of CMEs introduced by Subramanian *et al.* (1999) which contains their "creates streamer" and "displaced from streamer" categories has nothing to do with our population of CMEs that are not associated with any streamer. As pointed out in our analysis, this population is dominated by the faintest events and consequently was not detected neither by Hundhausen (1993) due to the poor quality of the SMM synoptic maps nor by Subramanian *et al.* (1999) probably due to a lower quality of their LASCO synoptic maps compared to ours and to relying on the visual detection of CMEs.

Excluding this population of CMEs that are not associated with any streamer, we have found that approximately 95 % of the remaining population of CMEs did experience a change and this percentage can be compared to those of Hundhausen (1993) who concluded that approximately 50 % of the CMEs observed in 1984 resulted in streamer disruptions and of Subramanian *et al.* (1999) who detected an effect for 54 % of CMEs. Here again, the same arguments concerning the quality of the different synoptic maps can be invoked as our high resolution and photometrically accurate maps certainly facilitate the detection of more modest changes. Contrary to the conclusions of Subramanian *et al.* (1999) who were puzzled by the large percentage of CMEs (46 %) that do not affect the streamer despite being associated with it, we have found that our result is consistent with the prevalent perception of widespread CME-streamer interactions.

Regarding changes induced by CMEs that imply a reconfiguration of the large-scale magnetic field, the dominating process is deviation, especially for the "top-ten" (70 %), followed by emergence/disappearance although these events are less numerous. We have noticed that deviations are mostly of two kinds:

i) temporary deviations, of small amplitudes, with the post-event streamer going back to the pre-event latitude in a few hours and

ii) permanent deviations with the post-event streamers remaining stable at its next location for many days.

As hinted at in the introduction, this tends to indicate that the views of Sime (1989) and Low (1996, 1997, 2001) that basically correspond to the above two kinds of deviation are not contradictory but reflect the reality of the different processes contributing to the reconfiguration of the coronal field. Whether the combined action of the CMEs is sufficient to remove the old magnetic flux and helicity from the corona to make room for the flux of the new cycle remains, however, an open question, which will require significant quantitative work to be ascertained.

References

Antiochos, S.K., DeVore, C.R., Klimchuk, J.A.: 1999, *Astrophys. J.* **510**, 485. doi:10.1086/306563.

Boursier, Y., Lamy, P., Llebaria, A., Robelus, S.: 2006, *SOHO-17. 10 Years of SOHO and Beyond, ESA SP-617*, 119.1 (in CDROM). doi:10.1007/s11207-009-9370-5.

Boursier, Y., Lamy, P., Llebaria, A., Goudail, F., Robelus, S.: 2009, *Solar Phys.* **257**, 125. doi:10.1007/s11207-009-9370-5.

Brueckner, G.E., Howard, R.A., Koomen, M.J., Korendyke, C.M., Michels, D.J., Moses, J.D., *et al.*: 1995, *Solar Phys.* **162**, 357. doi:10.1007/BF00733434.

Cho, K.S., Bong, S.C., Moon, Y.J., Shanmugaraju, A., Kwon, R.Y., Park, Y.D.: 2011, *Astron. Astrophys.* **530**, 16. doi:10.1051/0004-6361/201015578.

Dougherty, E.R.: 1992, *An Introduction to Morphological Image Processing*, SPIE Optical Engineering Press, Bellingham, 334 – 347.

Floyd, O., Lamy, P., Boursier, Y., Llebaria, A.: 2013, *Solar Phys.* doi:10.1007/s11207-013-0281-0.

Hiei, E., Hundhausen, A.J., Sime, D.G.: 1993, *Geophys. Res. Lett.* **20**, 2785. doi:10.1029/93GL01449.

Howard, R.A., Sheeley, N.R. Jr., Michels, D.J., Koomen, M.J.: 1985, *J. Geophys. Res.* **90**, 8173. doi:10.1029/JA090iA09p08173.

Hundhausen, A.J.: 1987, In: Pizzo, V.J., Holzer, T., Sime, D.G. (eds.) *Proceedings of the Sixth International Solar Wind Conference, NCAR Technical Note NCAR/TN-306* **2**, 181.

Hundhausen, A.J.: 1993, *J. Geophys. Res.* **98**, 13177. doi:10.1029/93JA00157.

Illing, R.M.E., Hundhausen, A.J.: 1986, *J. Geophys. Res.* **91**, 10951. doi:10.1029/JA091iA10p10951.

Lamy, P., Llebaria, A., Quemerais, E.: 2002, *Adv. Space Res.* **29**, 373. doi:10.1016/S0273-1177(01)00599-3.

Lin, J., Forbes, T.G.: 2000, *Bull. Am. Astron. Soc.* **32**, 842.

Liu, Y.: 2009, In: Lites, B., Cheung, M., Magara, T., Mariska, J., Reeves, K. (eds.) *The Second Hinode Science Meeting: Beyond Discovery – Toward Understanding*, ASP Conf. Ser. **415**, 152.

Llebaria, A., Saez, F., Lamy, P., Robelus, S., Boursier, Y.: 2006, *SOHO-17. 10 Years of SOHO and Beyond, ESA SP-617*, 135.1 (in CDROM).

Low, B.C.: 1983, In: Stenflo, J.O. (ed.) *Solar and Stellar Magnetic Fields: Origins and Coronal Effects*, Reidel Publishing Co., Dordrecht, 467.

Low, B.C.: 1996, In: Balasubramaniam, K.S., Keil, S.L., Smartt, R.N. (eds.) *Solar Drivers of the Interplanetary and Terrestrial Disturbances*, ASP Conf. Ser. **95**, 148.

Low, B.C.: 1997, In: Hansteen, V.H. (ed.) *Solar Magnetic Fields: Proceedings of a Mini-Workshop*, *University of Oslo*, 1.

Low, B.C.: 2001, *J. Geophys. Res.* **106**, 25141. doi:10.1029/2000JA004015.

Luhmann, J.G., Li, Y., Zhao, X., Yashiro, S.: 2003, *Solar Phys.* **213**, 367. doi:10.1023/A:1023939018916.

Mancuso, S., Raymond, J.C.: 2004, *Astron. Astrophys.* **413**, 363. doi:10.1051/0004-6361:20031510.

McAllister, A.H., Hundhausen, A.J.: 1996, In: Balasubramanian, K.S., Keil, S.L., Smartt, R.N. (eds.) *Solar Drivers of the Interplanetary and Terrestrial Disturbances*, *ASP Conf. Ser.* **95**, 171.

MacQueen, R.M., Hundhausen, A.J., Conover, C.W.: 1986, *J. Geophys. Res.* **91**, 31. doi:10.1029/JA091iA01p00031.

Mikic, Z., Linker, J.A.: 1994, *Astrophys. J.* **430**, 898. doi:10.1086/174460.

Odstrcil, D., Pizzo, V.J.: 1999, *J. Geophys. Res.* **104**, 493. doi:10.1029/1998JA900038.

Robbrecht, E., Berghmans, D., Van der Linden, R.A.M.: 2009, *Astrophys. J.* **691**, 1222. doi:10.1088/0004-637X/691/2/1222.

Saez, F., Llebaria, A., Lamy, P., Vibert, D.: 2007, *Astron. Astrophys.* **473**, 265. doi:10.1051/0004-6361:20066777.

Sime, D.G.: 1989, *J. Geophys. Res.* **94**, 151. doi:10.1029/JA094iA01p00151.

Subramanian, P., Dere, K.P., Rich, N.B., Howard, R.A.: 1999, *J. Geophys. Res.* **104**, 22321. doi:10.1029/1999JA900252.

Wolfson, R., Illing, R.M.E., Conover, C.: 1987, *J. Geophys. Res.* **92**, 13641. doi:10.1029/JA092iA12p13641.

Zhao, X., Hoeksema, J.T.: 1996, *J. Geophys. Res.* **101**, 4825. doi:10.1029/95JA03568.

Zuccarello, F.P., Bemporad, A., Jacobs, C., Mierla, M., Poedts, S., Zuccarello, F.: 2012, *Astrophys. J.* **744**, 66. doi:10.1088/0004-637X/744/1/66.